Northeast Journal of Complex Systems (NEJCS)

Volume 5
Number 1 *Special Issue: NERCCS 2023 Papers*

Article 3

June 2023

Temporality-induced chaos in the Kuramoto Model

Keanu Mason Rock
Toronto Metropolitan University, Toronto, Canada, keanu.mason.rock@torontomu.ca

Hamza Dirie
Toronto Metropolitan University, Toronto, Canada, hdirie@torontomu.ca

Sean P. Cornelius
Toronto Metropolitan University, Toronto, Canada, cornelius@torontomu.ca

Temporality-induced chaos in the Kuramoto Model

Keanu Mason Rock[1], Hamza Dirie[1], and Sean P. Cornelius[1,*]

[1] Toronto Metropolitan University, Toronto, Canada

[*] cornelius@torontomu.ca

Abstract

Switched dynamical systems have been extensively studied in engineering literature in the context of system control. In these systems, the dynamical laws change between different subsystems depending on the environment, a process that is known to produce emergent behaviors—notably chaos. These dynamics are analogous to those of temporal networks, in which the network topology changes over time, thereby altering the dynamics on the network. It stands to reason that temporal networks may therefore produce emergent chaos and other exotic behaviors unanticipated in static networks, yet concrete examples remain elusive. Here, we present a minimal example of a networked system in which temporality produces chaotic dynamics not possible in any static subnetwork alone. Specifically, we consider a variant of the famous Kuramoto model, in which the network topology alternates between different configurations in response to the phase dynamics. We show under certain conditions this can produce a strange attractor, and we verify the presence of chaos by analyzing its geometrical properties. Our results provide new insights on the consequences of temporality for network dynamics, and acts as a proof of concept for a novel mechanism behind generating chaotic dynamics in networks.

1 Introduction

Most studies of networked dynamical systems focus on what are called "static" networks, which have an immutable structure between nodes and links. In practice however, most real-world systems (*e.g.* ecosystems, human societies, and financial relationships) are naturally "temporal"—meaning that their structure changes over time [1, 2, 3]. It is now recognized that temporality can have profound effects on the dynamics of a system, for example enhancing network controllability [4], and fostering the emergence of cooperation in social systems [5, 6, 7]. But despite these

salutary examples, our understanding of the full effects of temporality on network dynamics is still in its infancy.

In its simplest form, we can regard a temporal network as a collection of static subnetworks or "snapshots", each representing the system's topology at a different times [8]. In many contexts, the change from one snapshot to another occurs in response to some dynamical process occurring on the network. For example, individuals in a social network may cut and reactivate social ties as a pandemic ebbs and flows [9, 10]. Likewise, in power systems, everything from line overloads to changing demand create a network that is constantly in flux. These forms of dynamics are well-studied in the engineering literature under the rubric of *switched dynamical systems* [11, 12, 13]. What implications might there be for temporal networks?

A surprising fact about switched systems is that they can produce exotic behaviors not possible in any subsystem alone. One particularly consequential example is chaos, which poses fundamental obstacles to the predictability of complex systems. Chaos is possible only in nonlinear systems, but it can curiously appear by switching between different *linear* systems.

Owing to their connection with switched systems, it's plausible that temporal networks may similarly exhibit chaos and other emergent behaviors relative to their static counterparts. But unfortunately, almost all examples of this phenomenon come from abstract piecewise linear systems [14, 15, 16, 17, 18, 19, 20]. As such, the possibility of temporality-induced chaos in networked systems of practical interest remains an open question.

In this manuscript, we provide a proof of principle showing how chaos can emerge from the addition of temporality to an otherwise mundane networked system. Specifically, we consider a network of Kuramoto oscillators, whose topology alternates between two different configurations (snapshots) depending on the state of the nodes, in turn changing their dynamics. We show that under certain conditions, chaotic dynamics can appear, despite being impossible in any static network snapshot by itself.

The rest of the paper is organized as follows: Section 2 introduces our temporal network dynamics, and the specific parameters used therein. Section 3 analyzes the dynamics of the individual snapshots, compared with the combined temporal dynamics in the presence of switching. We demonstrate that the latter system is chaotic, with a strange attractor characterized by a positive Lyapunov exponent and fractal Poincaré section. In section 4, we offer some concluding remarks and prospects for future work. Finally, details on our methodology can be found in Section 5.

2 Model

2.1 The Kuramoto Model

We consider the famous Kuramoto dynamics played out on a temporal network with N nodes. At any given time, the network's structure is described by one of M distinct static networks we call *snapshots*. The state of each node i is described by a phase angle θ_i, whose dynamics obey:

$$\dot{\theta}_i = \omega_i + \sum_{j=1}^{N} A_{ji}^{(\sigma(t))} \sin(\theta_j - \theta_i). \tag{1}$$

Here, $A^{(k)}$ is a weighted, directed adjacency matrix representing the topology of snapshot k, $A_{ji}^{(k)}$ represents the weight of the directed link $j \to i$ in that snapshot, and ω_i is the node i's natural frequency. Finally, $\sigma(t)$ is an integer-valued *switching signal*, where $\sigma(t) \in \{1, \ldots, M\}$ captures which of the M snapshots describes the network's topology at a given time t. We will allow for both positive and negative link weights in the snapshots, representing synchronizing and anti-synchronizing influences respectively. For simplicity, we set $\omega_i = 0$ for all nodes in order to focus exclusively on the dynamics resulting from the network interactions.

2.2 Model Parameters

Our goal is to show that temporality can produce chaotic dynamics even in the simplest cases. We therefore focus on only $M = 2$ snapshots, *i.e*, the minimal departure from the static network case ($M = 1$). We likewise consider only $N = 4$ nodes, which as argued below, corresponds to 3 dynamical degrees of freedom in the Kuramoto dynamics—the usual minimum required to observe chaos in an autonomous system. The adjacency matrices of the two specific snapshots we consider are

$$A^{(1)} = \begin{bmatrix} 0 & -1 & 0 & 0 \\ 1 & 0 & 0 & 0 \\ -0.1 & -0.1 & 0 & 0 \\ -1 & 1 & 0.25 & 0 \end{bmatrix} \tag{2}$$

and

$$A^{(2)} = \begin{bmatrix} 0 & -1 & 0 & 0 \\ 1 & 0 & 0 & 0 \\ 0.05 & 0.2 & 0 & 0 \\ -1 & 1 & -0.25 & 0 \end{bmatrix}, \tag{3}$$

and the corresponding directed networks are visualized in Fig. 1.

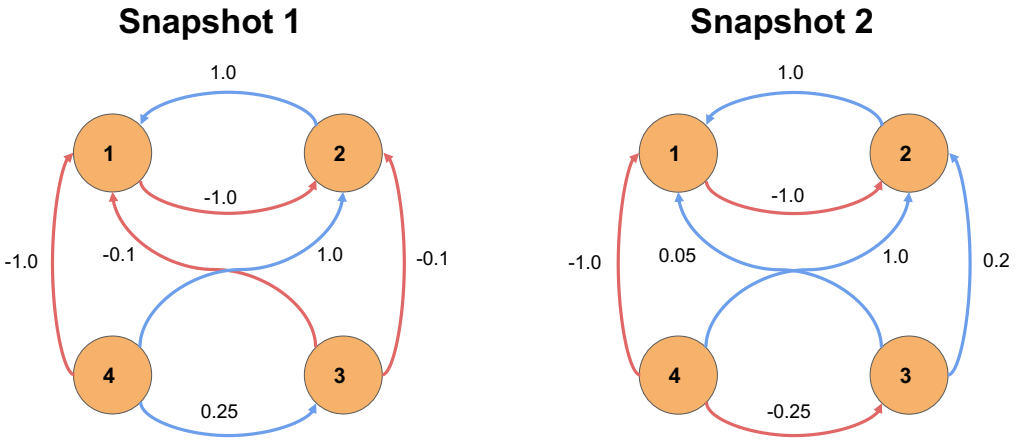

Figure 1 – Network Snapshots: Here, we visualize the two network snapshots comprising our temporal Kuramoto network. Arrows represent directed links $i \to j$, and the number beside each denotes the corresponding link weight A_{ij}. Each link is colored blue (red) based on whether the associated weight is positive (negative), representing a synchronizing (anti-synchronizing) influence of node i on the dynamics of node j.

3 Results

3.1 Dynamics of Individual Snapshots

First, we show that either snapshot of our network is incapable of producing chaotic dynamics on its own. In particular, we can show that all trajectories converge to a fixed point. As such, the emergence of chaotic dynamics (which we will explore later) can be attributed only to the addition of temporality. To prove this, we first investigate the long-term dynamics of each snapshot in isolation.

To start, note that we can always reduce the dimensionality of our system by measuring all nodes' phases relative to that of an arbitrarily chosen reference node, which we take as node 4 without loss of generality. Thus, after a transformation by $\theta_i \to \theta_i - \theta_4$, we arrive at a reduced, 3-dimensional system for each snapshot describing its standalone Kuramoto dynamics:

$$\begin{cases} \dot{\theta_1} = \sin(\theta_2 - \theta_1) - 0.1\sin(\theta_3 - \theta_1) + \sin(\theta_1) \\ \dot{\theta_2} = -\sin(\theta_1 - \theta_2) - 0.1\sin(\theta_3 - \theta_2) - \sin(\theta_2) \\ \dot{\theta_3} = 0.25\sin(\theta_3) \end{cases} \tag{4}$$

for snapshot 1, and

$$\begin{cases} \dot{\theta_1} = \sin(\theta_2 - \theta_1) + 0.05\sin(\theta_3 - \theta_1) + \sin(\theta_1) \\ \dot{\theta_2} = -\sin(\theta_1 - \theta_2) + 0.2\sin(\theta_3 - \theta_2) - \sin(\theta_2) \\ \dot{\theta_3} = -0.25\sin(\theta_3) \end{cases} \tag{5}$$

for snapshot 2.

By inspection, we see that in both snapshots, the 2D planes defined by $\theta_3 = n\pi$ are invariant for any integer n. Furthermore, between any adjacent pair of these planes, the dynamics of θ_3 is monotone. In particular, all trajectories in snapshot 1 (2) must asymptotically approach a plane $\theta_3 = n\pi$ defined by an odd (even) value of n. As such, as $t \to \infty$, the autonomous dynamics of either snapshot is effectively two-dimensional (in θ_1, θ_2). This observation already rules out the possibility of chaos in either snapshot alone, but we can gain further insight by analyzing the effective 2D dynamics of the snapshots in their respective limiting planes. Without loss of generality, we henceforth focus on the region of initial conditions $0 < \theta_3 < \pi$. There, all trajectories must approach the plane $\theta_3 = 0$ ($\theta_3 = \pi$) under the dynamics of snapshot 1 (snapshot 2). We denote these limiting planes by $P^{(1)}$ and $P^{(2)}$, respectively.

The limiting 2D dynamics of our snapshots in these planes is visualized in Fig. 2. Because our dynamics are invariant under translation of any θ_i by 2π, it suffices to focus on the subspace $-\pi \leq \theta_1, \theta_2 \leq \pi$. In this region, each snapshot has 11 fixed points in its corresponding limiting plane: nine corresponding to $\theta_1, \theta_2 \in \{-\pi, 0, +\pi\}$, and two more corresponding to the solutions of

$$\frac{\sin\theta_1}{\sin\theta_2} = -\frac{0.9}{1.1} \tag{6}$$

for snapshot 1, and

$$\frac{\sin\theta_1}{\sin\theta_2} = -\frac{0.8}{1.05} \tag{7}$$

for snapshot 2. In either case, $(\theta_1, \theta_2) = (\pi, 0)$ is the only stable fixed point (again, up to translation of any oscillator by 2π). Additionally for either snapshot $k = 1, 2$, we can identify an appropriate Lyapunov function $V^{(k)}$ on the corresponding limiting plane $P^{(k)}$, taking the form of a 4^{th}-order polynomial in $\{\sin(\theta_i), \cos(\theta_i)\}_{i=1,2}$ (See Section 5.2). It follows that no closed orbits (such as limit cycles) exist in either snapshot. Indeed, all initial conditions must approach a fixed point in the limiting plane $P^{(1)}$ (snapshot 1) or $P^{(2)}$ (snapshot 2), and except on a set measure zero, this will be the unique stable equilibrium $(\pi, 0)$ identified earlier.

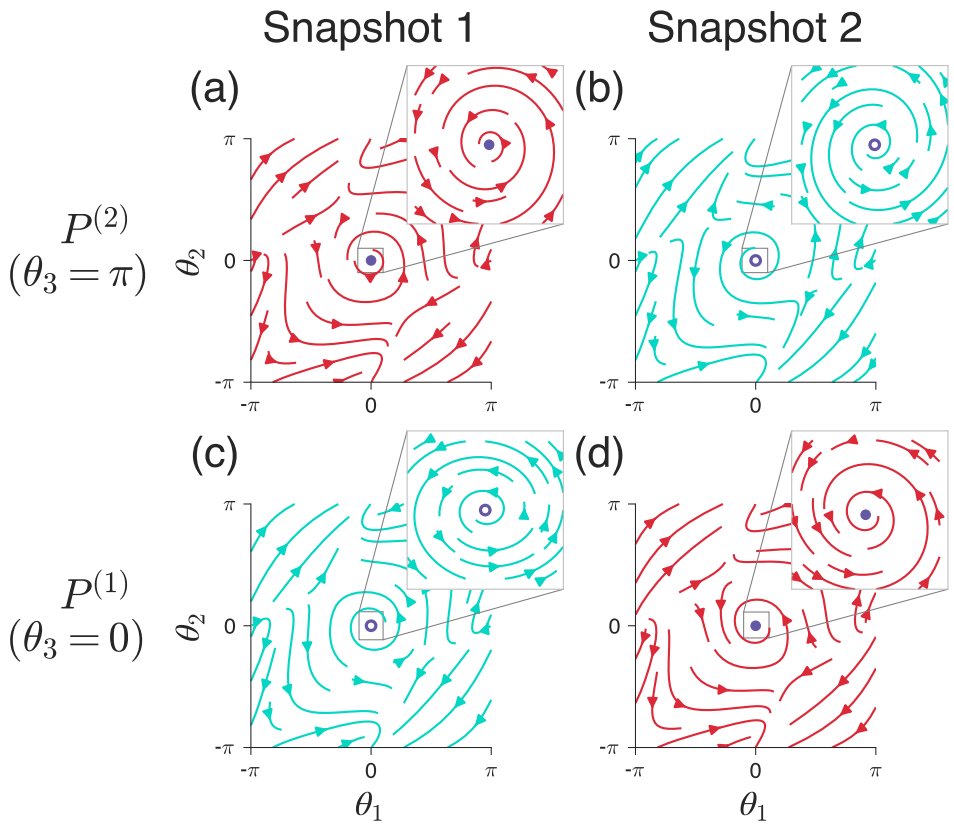

Figure 2 – Limiting Dynamics of Individual Snapshots: Here we show streamplots for the dynamics of snapshots 1 and 2 on the (θ_1, θ_2) plane at different values of θ_3. Specifically, $P^{(2)}$ (a and b) represents the $\theta_3 = \pi$ plane, and $P^{(1)}$ (c and d) represents the $\theta_3 = 0$ plane. In the vicinity of the origin, the dynamics of snapshot 1 spirals inward (red) in panel (a), and outward (blue) in panel (c), with these roles reversed in snapshot 2 (b,d). The stability of the fixed point at the origin is indicated by the purple circles, where filled and hollow represent stable and unstable respectively.

3.2 Temporal Dynamics and Strange Attractor

We incorporate temporality into our model via a *switching surface*—a specific subspace of our defined region that, when touched, swaps the network topology from one snapshot to the other. Specifically, we consider an approximately cylindrical surface around $(\theta_1, \theta_2) = (0, 0)$, *i.e.*:

$$\sin^2 \frac{\theta_1}{2} + \sin^2 \frac{\theta_2}{2} = r^2, \tag{8}$$

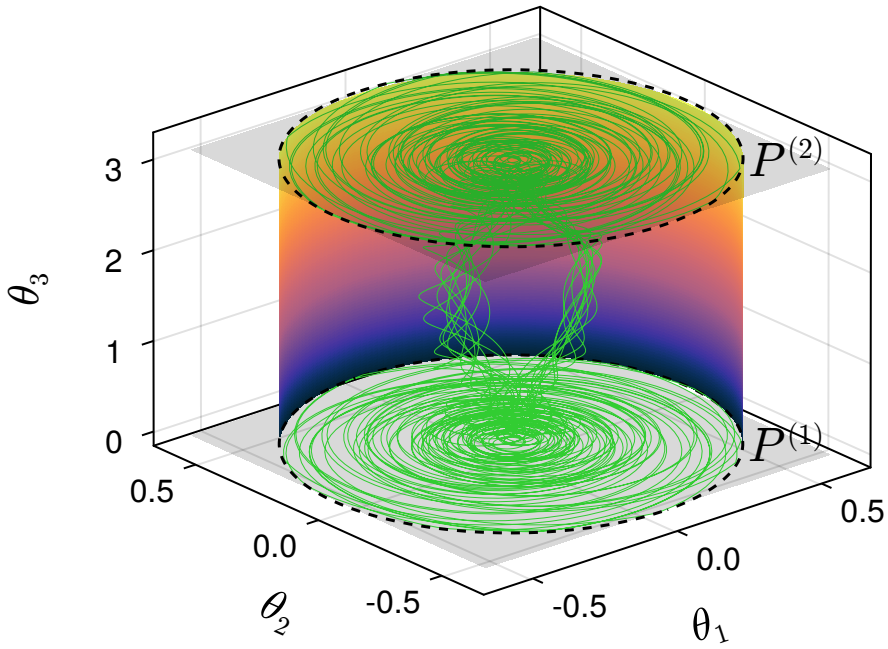

Figure 3 – Strange Attractor and Switching Surface. We show the strange attractor from our full temporal dynamics using an initial condition of $\theta_0 = [-0.101, 0.101, \pi - 0.101, 0]$, starting in snapshot 1 ($\sigma(0) = 1$) and integrated over 15,000 time units. The green curve represents the trajectory of our dynamics, while the dashed black line and gradient delineate our switching surface (Eq. 8). Whenever the trajectory touches this surface, the network topology switches to the other snapshot, causing the dynamics to spiral back inward. The result is a double-scroll attractor in which the dynamics shuttles unpredictably between the planes $P^{(1)}$ ($\theta_3 = 0$) and $P^{(2)}$ ($\theta_3 = \pi$), depicted in gray.

where $r > 0$ is a parameter. Throughout this study, we will use $r = 0.3$, though chaotic dynamics can appear across a range of r. Though ad hoc, this switching condition can be interpreted as the action of a controller tasked with keeping nodes 1 and 2 in phase synchrony with node 4 (Recall that in our coordinate system, $(\theta_1, \theta_2) = (0, 0)$ corresponds to $\theta_1 = \theta_2 = \theta_4$). Whenever those nodes' phases stray sufficiently far from the origin, the controller responds by changing the network topology to the other snapshot in which the origin is stable (cf. Fig. 2), thereby encouraging nodes 1 and 2 to synchronize.

The full temporal dynamics of our system is visualized in Fig. 3. We see that an apparently strange attractor emerges in the interior of the switching surface, comprised of vortex-like tendrils connecting two scroll "caps" located near the invariant planes $P^{(1)}$ and $P^{(2)}$. The appearance of this attractor, and the mechanism by which temporality generates chaos in this case, can be understood by examining the effective 2D dynamics of each snapshot and their interaction with our switching rule.

To see this, consider an initial condition in the interior of the switching surface, starting in snapshot 1. As argued earlier, the dynamics is drawn toward the plane $P^{(1)}$. Once there, the trajectory spirals outward from the origin (Fig. 2c), eventually touching the switching surface. At that instant, the dynamics switch to snapshot 2, under which the origin is now a *stable* spiral (Fig. 2d). As such, the trajectory is drawn back inward toward the origin, where it ultimately escapes along θ_3 toward snapshot 2's limiting plane ($P^{(2)}$). There, the origin is once again an unstable spiral (Fig. 2b), and the process repeats. As visualized in Fig. 3, this induces a family of unstable heteroclinic orbits between the fixed points at the origins in $P^{(1)}$ and $P^{(2)}$, which would not exist in the autonomous dynamics in either snapshot by itself. Indeed, the effect of temporality here is to frustrate the natural dynamics of each snapshot, always switching to the other before a stable fixed point (outside the switching surface) can be reached.

3.3 Poincaré Section and Largest Lyapunov Exponent

A strange attractor will generally reveal fine, fractal-like structure when subject to an appropriate Poincaré section. Here, we consider a surface of section defined by the plane $\theta_3 = \pi/2$, midway between the two scroll-like "caps" of the attractor. This cross section of is shown in Fig. 4, where a fine structure appears after many intersections. The apparent fractal structure indicates that the attractor shown in Figs. 3 and 4a is indeed strange, containing the dense collection of unstable heteroclinic orbits mentioned earlier.

We further confirm the presence of chaos in our system by numerically calculating the largest Lyapunov exponent (LLE, λ) of the strange attractor in Fig. 3, details of which can be found in the Methods (Sec. 5.3). We visualize the convergence of the LLE in Fig. 5, and find it approaches a value of $\lambda \approx 0.1952$ over time. The existence of a positive Lyapunov exponent reflects the exponential sensitivity to initial conditions suggested in Figs. 3-4, *i.e.* the signature of chaotic dynamics. We have confirmed that a positive LLE persists over times many orders of magnitude greater than the timescales present in either snapshot's dynamics (eqs. (4)-(5)), in order to rule out the possibility of chaotic transient.

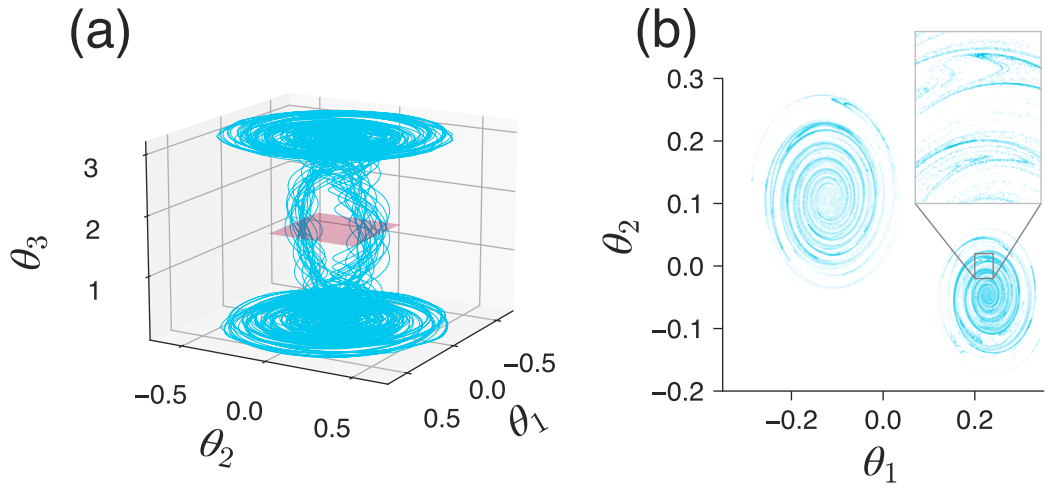

Figure 4 – Poincaré Section: (a) The strange attractor generated by our temporal dynamics using the same initial condition seen in Fig. 3, over a longer time of 2,400 seconds. The plane at $\theta_3 = \pi/2$ (red) indicates the surface at which we compute our Poincaré section. In (b), we show all points at which the attractor crosses this plane over 10^6 time units, resulting in approximately 220,000 intersections. The fractality present in the Poincaré section is highlighted in the inset of (b).

4 Conclusions

In this study, we have presented a minimal proof of principle showing how temporality (and temporality alone) is sufficient to produce chaos in network dynamics. In particular, by switching between two different Kuramoto networks a strange attractor can emerge, characterized by a positive Lyapunov exponent ($\lambda \approx 0.1952$), and showing characteristic fractal-like structure under a Poincaré section. This, to our knowledge, is the first example of chaos arising from temporality in a canonical networked dynamical system, and hints at a more general mechanism behind the emergence of chaos in co-evolving systems. Although chaotic dynamics have previously been produced in Kuramoto systems via continuously-varying network parameters [21], our work is distinct in that we produce chaos through switching between different network topologies.

The Kuramoto model was designed as a workhorse model of phase/frequency synchronization, but is nonetheless capable of producing far more exotic behaviors. Notable among these are "chimera states"—a form of symmetry-breaking in which identical oscillators self-organize into phase-locked and decoherent subsets that coexist with one another. In finite networks, chimera states can in fact be viewed as a form of (transient) chaos [22, 23, 24, 25]. Here, we have shown that similarly rich

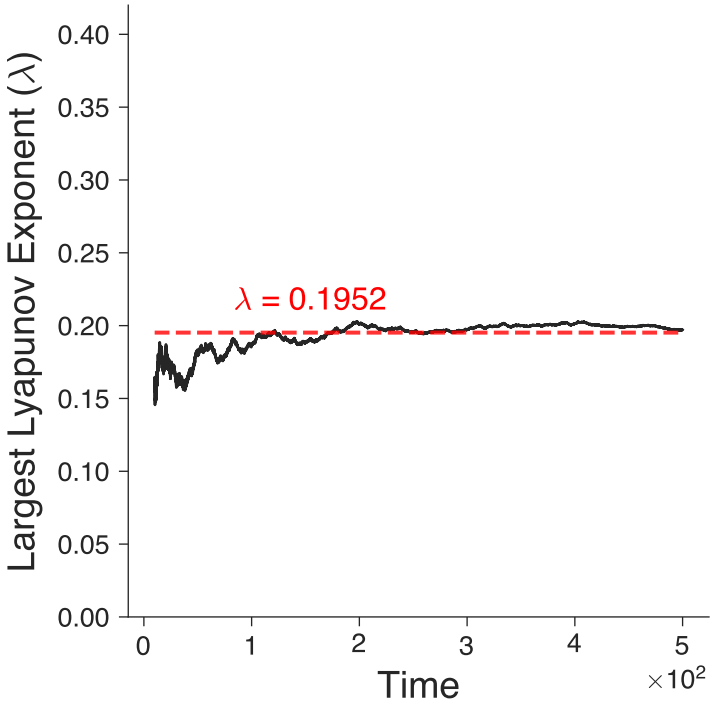

Figure 5 – Largest Lyapunov Exponent: The black curve represents our numerical estimate of the largest Lyapunov exponent (LLE) up to a given amount of simulation time. Specifically, each point represents the cumulative average (up to the given time) of local LLE estimates calculated over time windows of $\Delta t = 0.1$ (see Sec. 5.3 for details). We find that the LLE converges to a positive value, confirming the presence of chaos. The long-term average of $\lambda \approx 0.1952$ (red line) was computed over 1.5×10^6 time units. Here, we depict only the first 500 time units to show convergence.

and counterintuitive behaviors are possible when one adds temporality to the picture. In particular, one can create a chaotic Kuramoto system from two non-chaotic ones. We expect this construction to be possible in real-world systems such as power grids and communications networks, which can be governed by Kuramoto-like dynamical laws [26, 27] and also exhibit temporality in various forms.

The possibility of temporality-induced chaos has significant implications for practical applications of networks, particularly in engineered systems. Though chaos can be seen as desirable in certain biological contexts including neuronal dynamics [28, 29], it is generally a nuisance in built systems, which are often designed to operate in predictable steady states. In power-grid networks for example, normal operation corresponds to all generators operating in a state of frequency synchrony [30], deviations from which have been implicated in major blackouts

[31, 32]. Accordingly, future research should seek to identify and anticipate the exact circumstances (*e.g* switching conditions, link weights, dynamics, etc.) in which temporality is capable of producing chaos and other potentially undesirable dynamics. This may ultimately lead to new methods to control temporal systems, allowing us to harness their demonstrated benefits [4, 7] while avoiding unintended consequences.

5 Methods

5.1 Software Implementation

All simulations in this study were performed in Julia using the `DifferentialEquations` package. To obtain trajectories of our system, we integrate the equations of motion using a 9th-order adaptive integration scheme (Vern9) with absolute and relative error tolerances both set to 10^{-12}. We avail ourselves of the event-handling functionality of `DifferentialEquations` to implement the switching condition defined in Eq. 8, as well as generate the Poincaré section shown in Fig. 4.

5.2 Lyapunov Function via Sum-of-squares

We identify a sum-of-squares Lyapunov function for each snapshot's dynamics using MATLAB's `SOSTOOLS` package for semi-definite programming [33]. This technique can only be applied to polynomial systems, and so we consider each subsystem (Eqn. 4-5) restricted to its corresponding limiting plane $P^{(1)}$ or $P^{(2)}$, and re-express the dynamics in terms of the variables

$$\begin{cases} u_1 = \sin(\theta_1) \\ u_2 = \sin(\theta_2) \\ v_1 = \cos(\theta_1) \\ v_2 = \cos(\theta_2). \end{cases} \tag{9}$$

This yields an equivalent polynomial system of ODEs in 4D, subject to the constraints that the phases lie on the unit circle *i.e.*

$$u_i^2 + v_i^2 = 1. \tag{10}$$

For each snapshot $k = 1, 2$, `SOSTOOLS` successfully identifies a 4^{th}-order polynomial function $V^{(k)}(u_1, u_2, v_1, v_2)$ that, under the snapshot's dynamics, decreases everywhere except at the fixed points in $P^{(k)}$, attaining a global minumum at $(\pi, 0)$. Accordingly, $V^{(k)}$ acts as a Lyapunov function for snapshot k, proving that fixed

point's (almost) global stability. For reasons of space and clarity, we do not include the explicit form of either Lyapunov function here.

5.3 Lyapunov Exponent

We calculate the largest Lyapunov exponent (LLE) via the standard numerical approach [34], measuring the average exponential rate of separation of nearby trajectories. Specifically, we consider two initial conditions separated by a small Euclidean distance $d_0 = 10^{-8}$. After evolving both by $\Delta t = 0.1$ time units, we calculate a (local) estimate of the LLE according to

$$\lambda_i = \frac{\log \frac{d_1}{d_0}}{\Delta t},$$

where d_1 is the separation between the trajectories after evolution. We then renormalize the distance be between the trajectories to again be d_0, and repeat the process for a total of T iterations. The LLE is then calculated as the long-term ($T \gg 1$) average of the local estimates, *i.e.*:

$$\lambda = \frac{1}{T} \sum_{i=1}^{T} \lambda_i.$$

We stress that we regard the two trajectories as independent copies of the dynamical system under study, meaning they can reach the switching surface (Eqn. 8)—and hence, switch between network snapshots—at slightly different times.

References

[1] Jason M. Tylianakis and Rebecca J. Morris. Ecological Networks Across Environmental Gradients. *Annual Review of Ecology, Evolution, and Systematics*, 48(1):1–24, 2016.

[2] Longfeng Zhao, Gang-Jin Wang, Mingang Wang, Weiqi Bao, Wei Li, and H. Eugene Stanley. Stock market as temporal network. *Physica A: Statistical Mechanics and its Applications*, 506:1104–1112, 2018.

[3] Daniel Charbonneau, Benjamin Blonder, and Anna Dornhaus. Temporal Networks. *Understanding Complex Systems*, pages 217–244, 2013.

[4] A. Li, S. P. Cornelius, Y.-Y. Liu, L. Wang, and A.-L. Barabási. The fundamental advantages of temporal networks. *Science*, 358(6366):1042–1046, 2017.

[5] David Melamed, Ashley Harrell, and Brent Simpson. Cooperation, clustering, and assortative mixing in dynamic networks. *Proceedings of the National Academy of Sciences of the United States of America*, 115(5):951–956, 2018.

[6] David G. Rand, Samuel Arbesman, and Nicholas A. Christakis. Dynamic social networks promote cooperation in experiments with humans. *Proceedings of the National Academy of Sciences*, 108(48):19193–19198, 2011.

[7] Aming Li, Lei Zhou, Qi Su, Sean P Cornelius, Yang-Yu Liu, Long Wang, and Simon A Levin. Evolution of cooperation on temporal networks. *Nature communications*, 11(1):2259, 2019.

[8] Fabíola S.F. Pereira, Sandra de Amo, and João Gama. Evolving Centralities in Temporal Graphs: A Twitter Network Analysis. *2016 17th IEEE International Conference on Mobile Data Management (MDM)*, 2:43–48, 2016.

[9] Brennan Klein, Timothy LaRock, Stefan McCabe, Leo Torres, Lisa Friedland, Filippo Privitera, Brennan Lake, Moritz UG Kraemer, John S Brownstein, David Lazer, Tina Eliassi-Rad, Samuel V Scarpino, Alessandro Vespignani, and Matteo Chinazzi. Assessing changes in commuting and individual mobility in major metropolitan areas in the United States during the COVID-19 outbreak. *Northeastern University-Network Science Institute Report*, 2020.

[10] Brennan Klein, Timothy LaRock, Stefan McCabe, Leo Torres, Lisa Friedland, Filippo Privitera, Brennan Lake, Moritz UG Kraemer, John S Brownstein, David Lazer, Tina Eliassi-Rad, Samuel V Scarpino, Alessandro Vespignani, and Matteo Chinazi. Reshaping a nation: Mobility, commuting, and contact patterns during the COVID-19 outbreak. *Northeastern University-Network Science Institute Report*, 2020.

[11] Hai Lin and P.J. Antsaklis. Stability and Stabilizability of Switched Linear Systems: A Survey of Recent Results. *IEEE Transactions on Automatic Control*, 54(2):308–322, 2009.

[12] Daniel Liberzon. Switching in Systems and Control. *Systems & Control: Foundations & Applications*, 2003.

[13] Robert Shorten, Fabian Wirth, Oliver Mason, Kai Wulff, and Christopher King. Stability Criteria for Switched and Hybrid Systems. *SIAM Review*, 49(4):545–592, 2007.

[14] Maxim Poliashenko and Susan R. McKay. Chaos due to homoclinic and heteroclinic orbits in two coupled oscillators with nonisochronism. *Physical Review A*, 46(8):5271–5274, 1992.

[15] J. C. Chedjou, P. Woafo, and S. Domngang. Shilnikov Chaos and Dynamics of a Self-Sustained Electromechanical Transducer. *Journal of Vibration and Acoustics*, 123(2):170–174, 2001.

[16] R. J. Escalante-González, E. Campos-Cantón, and Matthew Nicol. Generation of multi-scroll attractors without equilibria via piecewise linear systems. *Chaos: An Interdisciplinary Journal of Nonlinear Science*, 27(5):053109, 2017.

[17] R J Escalante-González and Eric Campos. Multistable Systems with Hidden and Self-Excited Scroll Attractors Generated via Piecewise Linear Systems. *Complexity*, 2020:1–12, 2020.

[18] Tidjani Menacer, René Lozi, and Leon O. Chua. Hidden Bifurcations in the Multispiral Chua Attractor. *International Journal of Bifurcation and Chaos*, 26(14):1630039, 2016.

[19] Juan Gonzalo Barajas-Ramírez, Arturo Franco-López, and Hugo G. González-Hernández. Generating Shilnikov chaos in 3D piecewise linear systems. *Applied Mathematics and Computation*, 395:125877, 2021.

[20] Ning Wang, Chengqing Li, Han Bao, Mo Chen, and Bocheng Bao. Generating Multi-Scroll Chua's Attractors via Simplified Piecewise-Linear Chua's Diode. *IEEE Transactions on Circuits and Systems I: Regular Papers*, 66(12):4767–4779, 2019.

[21] Paul So and Ernest Barreto. Generating macroscopic chaos in a network of globally coupled phase oscillators. *Chaos: An Interdisciplinary Journal of Nonlinear Science*, 21(3):033127, 2011.

[22] Daniel M. Abrams and Steven H. Strogatz. Chimera States for Coupled Oscillators. *Physical Review Letters*, 93(17):174102, 2004.

[23] Simona Olmi. Chimera states in coupled Kuramoto oscillators with inertia. *Chaos: An Interdisciplinary Journal of Nonlinear Science*, 25(12):123125, 2015.

[24] Matthias Wolfrum and Oleh E. Omel'chenko. Chimera states are chaotic transients. *Physical Review E*, 84(1):015201, 2011.

[25] Christian Bick, Mark J. Panaggio, and Erik A. Martens. Chaos in Kuramoto oscillator networks. *Chaos: An Interdisciplinary Journal of Nonlinear Science*, 28(7):071102, 2018.

[26] Florian Dorfler and Francesco Bullo. Synchronization and Transient Stability in Power Networks and Non-Uniform Kuramoto Oscillators. *SIAM Journal on Control and Optimization*, 2009.

[27] Jorge Luis Ocampo-Espindola, Oleh E Omel'chenko, and István Z Kiss. Non-monotonic transients to synchrony in Kuramoto networks and electrochemical oscillators. *Journal of Physics: Complexity*, 2(1):015010, 2021.

[28] Megan Morrison and Lai-Sang Young. Chaotic heteroclinic networks as models of switching behavior in biological systems. *Chaos: An Interdisciplinary Journal of Nonlinear Science*, 32(12):123102, 2022.

[29] Henri Korn and Philippe Faure. Is there chaos in the brain? II. Experimental evidence and related models. *Comptes Rendus Biologies*, 326(9):787–840, 2003.

[30] Paul M Anderson and A A Fouad. Power System Control and Stability. 2002.

[31] G. Andersson, P. Donalek, R. Farmer, N. Hatziargyriou, I. Kamwa, P. Kundur, N. Martins, J. Paserba, P. Pourbeik, J. Sanchez-Gasca, R. Schulz, A. Stankovic, C. Taylor, and V. Vittal. Causes of the 2003 major grid blackouts in North America and Europe, and recommended means to improve system dynamic performance. *IEEE Transactions on Power Systems*, 20(4):1922–1928, 2005.

[32] Ian Dobson, Benjamin A. Carreras, Vickie E. Lynch, and David E. Newman. Complex systems analysis of series of blackouts: Cascading failure, critical points, and self-organization. *Chaos: An Interdisciplinary Journal of Nonlinear Science*, 17(2):026103, 2007.

[33] A. Papachristodoulou, J. Anderson, G. Valmorbida, S. Prajna, P. Seiler, and P. A. Parrilo. *SOSTOOLS: Sum of squares optimization toolbox for MATLAB*. `http://arxiv.org/abs/1310.4716`, 2013. Available from `http://www.eng.ox.ac.uk/control/sostools`, `http://www.cds.caltech.edu/sostools`, `http://www.mit.edu/~parrilo/sostools`.

[34] Giancarlo Benettin, Luigi Galgani, and Jean-Marie Strelcyn. Kolmogorov entropy and numerical experiments. *Physical Review A*, 14(6):2338–2345, 1976.